

Development of a Multi-Position Nanoindentation Sample Mount for Biomechanical Characterization of Whole Human Corneal Tissue Mimicking Physiological Conditions

B. Sc. Bero Bressler

Abstract—Nanoindentation, also referred to as Bioindentation is used to characterize soft bio-material's bio-mechanics and mechanobiologic properties allowing for mapping representations of samples inhomogeneity. The tissue properties and characteristics of corneal tissue, as well as all other biological tissues, are extremely dependent on environmental influences. At present, the nanoindentation of whole corneal tissue under mimicked physiological conditions is not possible but necessary. Therefore a sample mount was designed enabling Bioindentation measurements of whole human corneal tissue under approximately physiological conditions.

The sample mount's essential function is to allow for multi-position immersed indentation of cell medium immersed whole human corneal tissue for bio-mechanical tissue characterization. While maintaining their natural shape, corneal indentations are enabled in the central, para-central and peripheral areas allowing for exertion of variable retro-corneal pressures or volume flow. The requirements, principal functionality, prototype evaluation and measurements regarding this novel approach are presented in this work. The latter performed study is showing a significant increase in elastic modulus in all characterized samples after collagen cross-linking therapy. After discussing the results and the evaluation of the designed sample mount, the paper concludes on the findings and lies out the scientific potentials of the development.

Index Terms—Nanoindentation, Bioindentation, Cornea, Sample Mount, Collagen Cross-Linking

I. INTRODUCTION

A. Nanoindentation Principles

NANOINDENTATION, due to its high spatial resolution and force sensitivity, has recently become particularly relevant for measuring mechanical properties of soft bio-materials.

It enables the localised understanding of bio-mechanics and mechanobiology as it offers significant region-specific mapping possibilities of bio-materials' inhomogeneity. The principle setup is shown in fig. 1 explaining its functionality. Compared to traditional test methods with a single measurement mode, indentation testing can provide an ideal loading modality that includes stress and strain fields as well

B. Bressler is a student in the Medical Technologies Master program at MCI Innsbruck, Austria. E-Mail: bero.bressler@mci4me.at

Special thanks go to the Thesis' supervisor PD Dr. S. Lang and the laboratory manager Prof. Dr. G. Schlunck for their support and assistance.

The author would also like to thank M.Sc. R. Lohmueller for the excellent induction and the workshop manager P. Weisert for outstanding technical support.

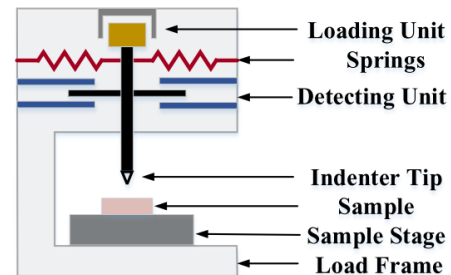


Fig. 1: Schematic nanoindenter representation and general components. During a typical test, the exerted force, depth of indentation and the time are monitored while the indenter is pressed onto the specimen. The response curve is fitted to a number of different constitutive models to determine the mechanical properties of the sample. Image taken from Qian et al. 2018 [1].

as tension, compression and shear loading modes and allows even the utilization of valuable samples like fossils [1]. Not only load capacity aspects but also other bio-functionalities are well known to be influenced by mechanical behaviour [2], such as the main biological functionalities, mechanisms, and diseases which are associated with the mechanical response at the bio-molecular and organ level as shown by e.g. [3][4][5]. If biological samples are used, nanoindentation is also referred to as bioindentation.

B. Aim and Necessity of the Sample Mount Development

The shape of the cornea is crucial for its optical properties and visual acuity. Keratoconus or other ectatic diseases are associated with distinct changes in shape such as protrusion and thinning of the corneal tissue. These changes in the natural shape of the cornea are probably due to the loss of stability leading to pathologically altered biomechanical properties of the corneal tissue. Due to these often progressive pathological changes in the shape, also the refractive power of the cornea, the visual acuity of the usually still young patients deteriorates drastically. Thus, reproducible measurements of corneal stiffness are essential for the evaluation of novel treatment regimens for keratoconus and other eye diseases. In the current protocols, dissected tissue samples are glued to a substrate for indentation, distorting shape and mechanical load

of the tissue, thereby rendering results of limited biological relevance [6], [7].

This works sample holder is intended for reproducible, immersed bioindentation measurements for the characterisation of whole cornea samples in natural shape with exertion of variable retrocorneal pressures to mimic physiological conditions and to allow for locally resolved mapping functionality.

C. Biomechanical Characterisation of Corneal Tissue

The cornea can be considered a soft tissue. Although in fact, the terms "hard" and "soft" say nothing about hardness or plastic deformation properties. Soft biomaterials implying only the non-mineralised state under healthy condition [8]. Soft biomaterials, such as globular proteins, cancer cells, arteries, cartilage and the brain, vary very much depending on the scale: from the molecular to the cellular and tissue to the organ level, the aforementioned complex hierarchical structures show differences, which requires diversified characterisation [1]. Being much more limber than typical engineering materials, several substantial models for mechanical description of soft biomaterials are widely used which are e.g. the hyperelastic, linear elastic, viscoelastic and poroelastic model. Numerous soft biomaterials show a nonlinear stress-strain behaviour which is shown in fig. 2a.

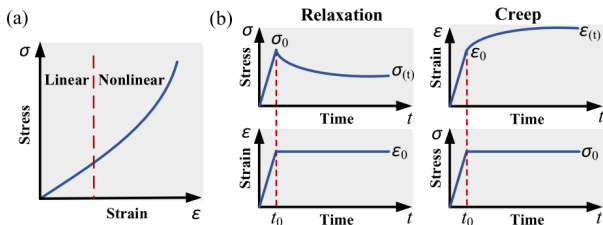


Fig. 2: Constitutive soft biomaterials response (a) Nonlinear stress-strain behavior; The initial linear section shows an increase in stress that is proportional to the strain for minor deformations but the stress increases progressively for higher strains and major deformations. Depending on the test method and the different biomaterials, the threshold for the linear range varies [9]. Dividing the stress profile into several sections is another strategy to simplify the nonlinear behaviour. The mechanical behaviour in each section can be considered linear and characterised using the linear elastic model. (b) time-dependent mechanical behaviour - stress-relaxation & creep. Image taken from Qian et al. [1].

An other particularity of soft biomaterials is their time-dependent mechanical behaviour is viscosity. For their characterization viscoelastic models are used to display a combination of elastic and time-dependent responses. "A viscoelastic material stores and dissipates mechanical energy simultaneously undergoing imposed mechanical excitation, with the response of stress-relaxation or creep over time" [1] which is shown in fig. 2b. For the evaluation and determination of the elastic modulus of corneal tissue, the Hertz formula is frequently used [10],[11],[12],[7]:

$$F = \frac{4}{3} \cdot E \cdot \sqrt{R} \cdot h^{\frac{3}{2}} \quad (1)$$

with the indentation depth h , spherical indenter radius R , elastic modulus E and the maximum load F during indentation.

Nonlinear viscoelasticity can be modeled on indentation. Another relevant soft biomaterial property resulting from its poroelastic and hydrated structures is also referred to as the "biphasic model", which is combining the two aforesaid attributes: the time-depending behaviour under physiological conditions describes the passing of a fluid through a porous elastic solid which leads to a fluid outflow under application of pressure. Prominent parameter to indicate the coupling of fluid and solid as well as the fluid flow is the Darcy permeability [13]. Swain et al showed this phenomenon for cornea tissue [6]. Considering this, the hydration state of the sample is an important factor influencing the mechanical characterisation of aqueous samples. Many different studies have obtained lower elastic modulus for hydrated soft biomaterials than for corresponding dry samples. The determined deviation can lie in an order of magnitude [1].

II. METHODS

A. Requirements Management Approach

Firstly, the underlying problem is analyze to understand the problem to be solved. To do so, in this development process the user and application requirements were collected. Secondly, the system requirements were derived. For the exchange of expectations and demands, a group of experts with different backgrounds, expertise and perspectives is formed consisting of Prof. Dr. G. Schlunck, PD Dr. S. Lang, M.Sc. R. Lohmüller and the author of this work. Within the group the problem is analysed by discussing different aspects in terms of user-oriented handling, functionality, biological and physical aspects. Resulting in the definition and formulation of user and application requirements. These do not necessarily have to be quantitative and are based on expert opinions, observations, and experiences as well as the existing scientific knowledge. The derived system requirements were prioritised according to their importance and fall into optional or mandatory criteria, where the latter shall be implemented thoroughly. In the course of development, according to prevailing possibility and needs, the requirements are not considered a static list but are to be extended or adapted to improve the overall outcome as shown in fig. 3. As shown in III-A, this document focuses exclusively on the mandatory requirements for the sake of clarity.

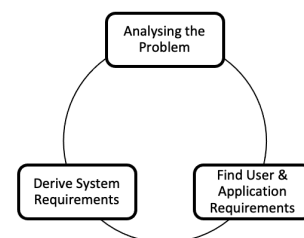


Fig. 3: Cyclical requirements management.

B. Concept Generation, Prototyping and Evaluation Methodology

To find technical solutions potentially satisfying the defined requirements, different ideas and concepts were gathered in an array of concept design alternatives. From this array a final design concept was selected afterwards. After the finding of different concepts, the most promising option shall be selected for further steps by means of a utility value analysis.

After deciding on the favoured concept, a specific design was created. Therefor the CAD modeling, manufacturing, product assembly and technical evaluation by testing the prototype was performed, in order to find aspects for improvement from flaws and usability issues. To do so, several materials and methods were used which are presented in the following. For the mechanical model design, Autodesk Inventor 2021 CAD software was used and a holistic assembly approach was chosen featuring all essential superstructure's components. As key element, the cornea was modeled according to the expert literature measurements and OCT data as explained in III-B. In this way, the constrains and technical relationship between the different sample mount's elements can be visualized and analyzed to determine angles or lengths respectively as presented in fig. 10. Also movements were simulated and analysed at the mechanical-technical level as well as height depending indentation deviations.

The materials and manufacturing techniques were selected on the price to performance ratio, availability and time to completion which is why the designed prototype was 3d printed and reworked by the workshop manager. A Formlabs Form 3 printer, belt grinder, CNC milling machine or lathe to remove support structure and produce true to size parts. The threads for the various spring loaded thrust pieces were cut and vacuum compensation holes for 3d printing were sealed with two-component adhesive.

By means of basic functionality test the general principles of the intended technical functionality is analyzed. The usability is assessed by the observations of a third party user. The findings from both methods are compared to the defined requirements and used to revise the modeled in order to improve its functionality as presented in section IV.

The following tests were defined to evaluate the sample mount: To check the possibility of haptic recognition of the four intended locking positions of the swing, the swing was mobilised by hand and brought into the various locking positions. Same procedure applies to the rotary element. Function check of the position adjustment of both elements by means of an Allen key. To determine the forces needed to change the swing position from the different locking positions, the structure was placed in the middle of a scale and the different positions were set. Six measurements were taken for each of the three tilted positions. The mass measurements grams were converted to weight in Newton, the mean value and standard deviation were calculated. The force was applied by hand with a single finger from a vertical direction with gradual addition of force and reading of the scale. To test the sealing property the container it was filled with water to a marked level close to the top and placed on hand drying paper for several hours.

The evaluation of usability and technical performance shall be analyzed, by observing the whole indentation procedure and indentation data evaluation, which is to be carried out by a third party and includes the execution of all required steps. Instead of a human donor cornea a contact lens is used and clamped into the chamber. The original silicone tubes shown in fig. 12 are extended with Luer-Lock connectors and tubes, a positive retrocorneal air pressure is applied using a typical syringe, the anterior chamber is inserted into the rotary element and is secured with screws. The container is filled with water for immersed indentation measurements.

C. Whole human cornea bioindentation before and after collagen cross-linking therapy

To collect preliminary model data in order to evaluate the possibility of immersed indentations of whole corneal tissue in an AAC with retrocorneal pressure, a simplified version of the sample mount was CAD modeled and printed where the rotation axes were omitted. The design uses the same modified artificial anterior chamber mount system, later referred to as "rotary element", as the sample mount and has an enclosing wall allowing for immersed indentation. Fifteen percent dextran cell medium was used to immerse the cornea. It is to be tested whether immersed measurements on a whole human cornea clamped in the artificial anterior chamber are possible at different retrocorneal pressure levels and if so, whether the treatment effects the indentation measurements. For this purpose, two controlled pressure levels are used for each of the $N = 3$ cornea samples to be characterized in its centre. First, a retrocorneal pressure is set to 20 mmHg for the 28 indentations and then the indentation is repeated with the pressure set to 40 mmHg. After that each cornea is cross-lined according to the conventional protocol using 370 nm UV light and 0.1 percent riboflavin. After the first indentations at the lower pressure, the measurements are repeated under the higher pressure condition. Therefor, the clamped cornea is mounted in a small container, which provides a clamping possibility with screw connections for the artificial anterior chamber mounting. This device was previously CAD modeled and 3d printed. This device has two holes for securing it to the Bioindenter's sample stage. The data was exported from the software and processed in the programming language R with R Studio (RStudio, Inc. Boston) for data plotting and statistical evaluation with paired sample wilcoxon tests of the obtained elastic modulus values obtained by the Hertzian fit.

III. RESULTS

A. Defined Requirements Overview

1) *Application and User Requirements:* The sample mount is to be designed as a reusable product and is not intended for series production. The size and height of the setup must be compatible with the use of the nanoindenter in the laboratory. To avoid costly repairs, special attention should be paid to avoid unwanted collisions of the superstructure with the tip of the Nanoindenter. The model in question is the UNHT³ from the manufacturer Anton Paar, a Bioindenter specially adapted to meet the requirements of soft, elastic specimen

allowing for immersed indentations using a spherical ruby tip. The bioindenter can determine elastic moduli of samples down to a stiffness of only 2 kPa. The use of whole corneas must be possible, for example by using an anterior chamber system such as Barron's Artificial Anterior Chamber, where fluids and gases can be applied for perfusion or to build up internal pressure via Luer-Lock adapters. The superstructure must allow the cornea to be fully immersed in dextran medium. There must be a solid and stable structure that is statically capable of withstanding the acting forces during indentation. The set-up must ensure fixed and reproducible indentation location according to the intended indentation matrix defining the areas of interest. It shall be possible to align the position

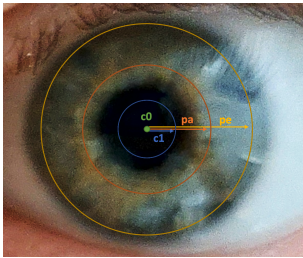


Fig. 4: Schematic of the regions to be tested. The radii are chosen to be about center in each region with the exception of the second radius in the central region which is located further outwards to prevent double measurement of the same location due to overlap from the intended indentation protocol.

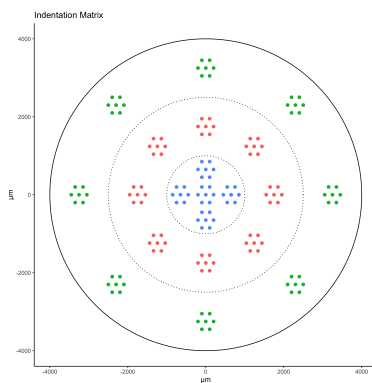


Fig. 5: Representation of the intended indentation matrix. At each of the 21 adjustable indentation locations, a surface detection (ADO adjust depth offset) is performed centrally and then the tissue is characterised with in this case six the ADO surrounding bioindentations using a spherical rubi. This makes 126 spatially resolved indentation measurements possible over the entire cornea.

fixed nanoindenter tip as orthogonal as possible to the cornea's surface for the various intended indentation locations. The avoidance of materials that may cause undesirable reactions with other components, materials or human corneal tissue to be used in the setup has to be ensured. Attention should be paid to the reusability of the set-up through cleanable and disinfected materials and durable components. Leakproof property of the components to be filled with medium must be

ensured in order to protect the nanoindenter from damage. The sample holder has to be safe, simple and intuitive to use. The fast and user-friendly assembly for measurement preparation is desirable as well as the readability of the respective set positions of the rotary axes, preferably also in the dark. A lid for the safe transport of the measurement set-up prepared in the laboratory to the site of the nanoindenter and a non-air-tight lid for storing the set-up in the incubator are required. The structure should be able to be manufactured and assembled in-house in a cost- and resource-saving manner. A

2) *Mandatory System Requirements*: This paragraph features the top prioritized system requirements which were derived from the previously presented application and user requirements. The requirements of lower priority are disregarded to focus on the essential aspects of the system emphasizing the technical design approach. First of all, a maximum height of 70 mm and a width or length of 130 mm must not be exceeded. All of the various desired corneal measurement points must be located no more than 7.5 mm lower than the highest point of the sample mount to ensure contact of the nanoindenter tip with the specimen without collision. Four different indentation radii were derived, which are the perpendicular distances to the corneal axis of rotation, are required. The radii are 0, 0.65, 1.75 and 3.25mm so that the measurements are about centre in each region as shown in fig. 4, where the first two radii refer to the central, the third to the paracentral and the fourth radius to the peripheral corneal region.

Positioning centred on cornea and firm fixation of the sample mount via a guide rail on the nanoindenter's sample stage with four M4 hexagon socket countersunk screws, with square 50 mm hole spacing are required. Secure clamping of a 14-18 mm corneal graft, including scleral band or scleral band section without rotation during clamping must be ensured. Two connections with crimp clamps for infusion or perfusion and pressure or flow application in the cornea interior via sufficiently long silicone tubes of 30 cm with Luer-Lock standard are required. The liquid impermeability of the area flooded with medium as well as a medium protrusion of 2mm must be guaranteed while assuring that excess filling resulting from interfacial tension must not lead to overflowing of the medium. Mechanical locking function for the measuring points on the four radii must exclude unintentional adjustment, is to be ensured by the use of simple components such as e.g. spring-loaded thrust pieces which do not require the use of tools. Orthogonality between the defined measurement sites and the NI apex as far as possible, taking into account the anatomy and the dimensions of the cornea according to the literature. The artificial anterior chamber must be tight enough to at least maintain internal pressures of physiological conditions around 20 mmHg for 30 minutes with minor drop in pressure or volume flow. The silicone tubes must be guided and securely fastened to the exterior of the superstructure for storage, transportation and during indentation measurements.

B. Comparison and Overview of the Considered Concepts

In total there were three concepts considered for potential implementation. In the following only two of them are briefly

presented in their structure and designated function. All concepts feature two orthogonal rotary axes that are designed to intersect with the high point of the cornea located on its rotation axis. To approach this requirement the cornea is considered to be clamped in and to remain in its original shape when it's mounted to the artificial anterior chamber. The concepts are based on a modified and height reduced version of Barron's artificial anterior chamber. With this, safe clamping and cornea handling according to III-A2 is possible. The cornea was modeled true to shape by the present expert literature measurements [14] and under the aid of an anterior segment OCT of a healthy human cornea in longitudinal section. Note that the consideration of the cornea as a turning part is disregarding the cornea's elliptical sphere. As the donated corneas are not orientation marked and the elliptical shape is enormously difficult to recognise even for trained personnel, the consideration of the elliptical shape in the model does not achieve any added value to the project. The CAD model of the cornea is represented as demonstrated in the fig. 6. For the implementation of the locking function at the desired positions, spring-loaded thrust pieces are frequently introduced, fig. 7 demonstrates their general concept.

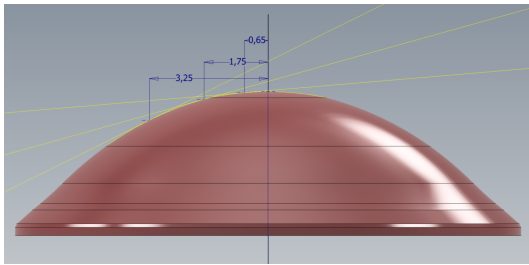


Fig. 6: Three-dimensional cornea model with contact points of interest [radii of 0, 0.65, 1.75 and 3.25 mm] and three yellow lines representing orthogonal planes onto the cornea surface.

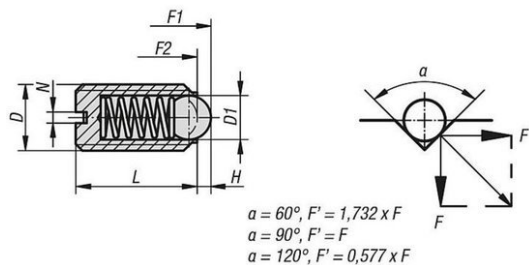


Fig. 7: Technical drawing (l) and functional illustration of the possible application of spring loaded thrust piece with a notch (r) and respective forces depending on the notch opening angle α . Image taken from [15]

1) *Gimbal Ring Design Concept:* Unlike the other concept, there is no rotation about the cornea's axis of rotation in the gimbal design concept. Therefore the artificial anterior chamber is mounted to a swing component which is sitting on the inside of the gimbal ring. To ensure the mountability of the swing element in the gimbal ring, a three-part swing was modeled, which can be inserted into the ring via two

dovetail connections. The ring again is mounted on the inside of the upper end of the liquid container supposed to be filled with medium for immersed indentation testing. By means of the independent rotation of the two perpendicular axes and fixation elements, such as spring-loaded pressure pieces, multiple indentation positions on the cornea can be realised. Screwed into the gimbal ring, appropriate arresting notches for the desired indentation positions are possible. Fig. 8 illustrates the here described concept and its components.

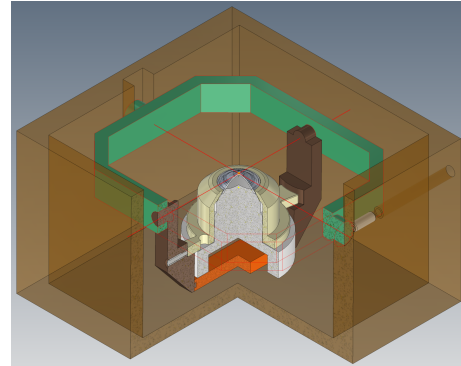


Fig. 8: Three-quarter section of the gimbal ring concept modeled in CAD. The rotary axes intersecting in the cornea's high point are shown in red.

2) *Swing and Rotary Element Design Concept:* Just like the previously presented, this concept combines two perpendicular rotational axes which intersect in the high point of the clamped cornea's rotary axis. Unlike the previously presented, this concept features one rotation axis, which is aligned with the cornea's axis of rotation. The artificial anterior chamber is not inserted directly into the swing, but on a rotary element allowing for rotation around the cornea's axis of rotation. A gimbal ring is dispensed with. Instead, the swing is inserted directly into the corresponding bearing component at the upper end of the liquid container. Four position lock spring loaded thrust pieces are intended to be placed in the swing and the walls of the fluid container. For a tidier appearance, these are not shown in fig. 9, but the symmetrical holes are recognisable.

C. Utility Analysis and Selection of a Concept for Detailed Implementation

Although the gimbal ring design appears small enough to fit beneath the Nanoindenter tip in the neutral position, the design is not meeting the previously set requirements. With regard to the height constraint II-A the gimbal ring swings out of the liquid container when adjusting the indentation location to the extremities. A collision with the Nanoindenter head will occur which is limiting the range of motion. This also means a serious threat to damage the Nanoindenter tip by accident. Proved to be an unsuitable design concept, the gimbal ring design was discarded for further considerations. This leaves only the swing and rotary element as well as the slider design for direct comparison and decision-making for one or the other.

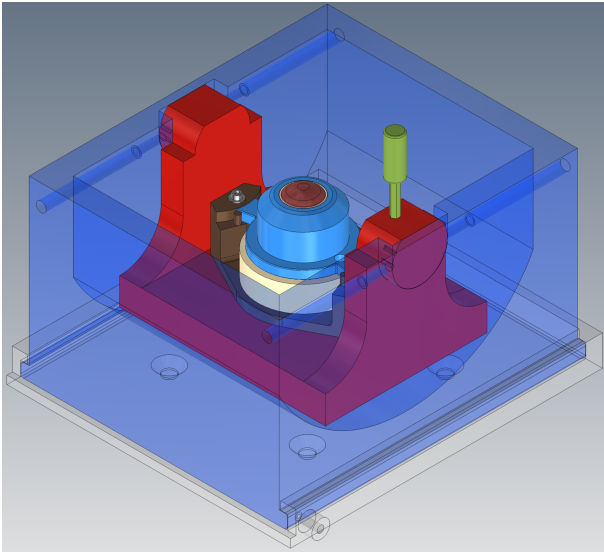


Fig. 9: Swing and rotary element design concept modeled in CAD featuring its basic components. Screws and locking devices are neglected.

The main advantage of the slider concept lies in the fact, that this design does not require any elements hanging from any components above the cornea's high point. As a result, the design tends to be more compact containing fewer components that build further upwards and thus endanger the nanoindenter tip. However, it also requires significantly more complex components, whereby the slider stands out in particular. Ideally, the radius of the slide rail should be exactly the same as the relative vertical height of the abutment to the high point of the cornea. It seems to require extraordinary measures resulting in high potential for procurement or manufacturing. Although the swing and rotary element design concept has more and further upward components, tip collision is still avoidable and the components are expected easily to be crafted with less effort resulting in fewer potential problems than with the slider design. As a conclusion, the swing and rotary element design concept was elected to be detailed and prototyped.

D. Detailed Description of the Elected Concept's Prototype and its Functional Components

This section is based on the swing and rotary element design concept presented in chapter III-B2 which was selected for prototyping according to the previous chapter III-C. It describes the detailed elements and aspects of the CAD modeled version shown in fig. 9. The prototype shown in fig. 12 was developed to evaluate the concept's functionality, detect flaws, derive new requirements and find new ideas for improvement which is later referred to in section III-E and IV and is discussed respectively.

1) *Guide rail:* The guide rail is the lowest component and is in direct contact to the Nanoindenter's sample stage. To be securely mounted, four M4 countersunk head screws are required. The lateral guides along the insertion axis were designed in a U-shape and the end opposite the insertion side was closed. The attachment of the medium filled container

does not require any tools for securely placing into the guide rail. A small protrusion of the bottom of the guide rail facilitates the insertion. As shown in fig. 9 at one side of the guide rail, there is a hole positioned transversely to the single-feed axis designated for an M5 spring-loaded thrust piece. When the container is fully inserted into the guide rail, the spring-loaded thrust piece engages with a pocket in the container to secure it in the guide rail as presented in fig. 7. To remove the container, a slight but precise exertion of force against the insertion axis is required to compress the spring and release the locking device.

2) *Container:* As already mentioned, the container can be securely fastened in the guide rail without the need for any tools. On one hand, the container fulfils the load-bearing function for the other parts of the body. On the other hand, it has the holes for holding the locking devices, which are required to adjust and lock the desired swing position. To support the other components, the container has two symmetrical recesses on two sides of the container, which are open at the top and rounded at the bottom. The upper opening enables insertion, whereas the lower pocket's rounding serves as a glide surface for the insertable swing element. To avoid suction forces while resin based 3d printing with the Formlabs Form 3 model, a ventilation hole was inserted in the model and sealed afterwards with two-component glue. So, it can be filled with medium to ensure an overlap with medium at the cornea. Fig. 9 illustrates the container with the swing element placed in it.

3) *Swing element:* The swing can rotate through about 27° degrees from neutral position where the absolute end points are defined by the stop on the container. The swing has two sliding surfaces that are designed a tenth smaller in diameter than the container's pockets to be inserted into the container and achieve minimal radial play. To prevent friction with the inner wall of the container when moving, the width of the swing was set 0.45 mm narrower than the container's width. To achieve a snug fit with minimal axial play the swing's sliding elements width was set a tenth smaller than the container's notch width. With notches constructed into the sliding surfaces of the tread element of the swing, the spring loaded thrust pieces sitting in the container's walls take over the locking function of the swing at the four defined positions. Here, two opposing spring loaded thrust pieces are used to lock one position. The notches have an opening angle of 90° which means that the locking force is ideally equal to the spring loaded thrust pieces force as shown in 7. Therefore, there are a total of eight notches on the swing. The notch angles to achieve perpendicular indentation to the cornea's surface on the defined radii according to 10 were found by means of the measuring tool in CAD assembly. For this purpose, the angles between the planes shown in fig. 6 and the horizontal plane in the neutral swing position shown in fig. 9 were measured. The angles from the horizontal for the four notch positions are presented in table I.

TABLE I: Configuration angles of the cornea for orthogonal indentation on the corresponding radii and respective Y-axis displacement

Configuration	Configuration Angle / °	Y-axis displacement / mm
C0	0	0
C1	4.8	0.65
Pa	15.6	1.74
Pe	26.3	3.26

Two of which are illustrated in fig. 10. They correspond to the second central Z1 and the peripheral locking position Pe. In the middle of the swing a hole for the rotation element is placed. From one side of the swing a horizontal hole for a spring loaded thrust piece is foreseen to lock the rotating element in one of the eight desired positions.

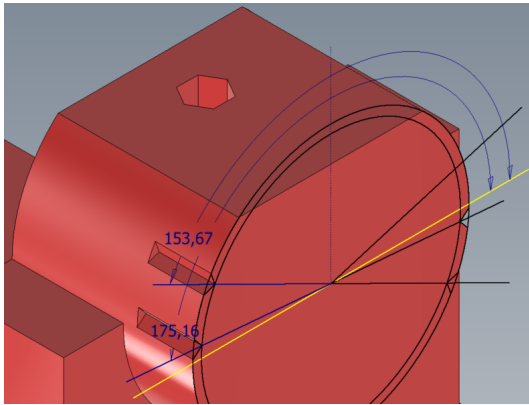


Fig. 10: CAD model of the swing's sliding element with the 2D sketch of angles for notch positioning ensuring for rectangular indentation angles at the cornea radii of 0.65 and 3.25 mm for second central position and periphery position corresponding to 4.8426° and 26.3307°. The yellow line corresponds to the horizontal plane and serves as a reference for the angle dimensioning.

4) *Rotary element*: The rotating element can be rotated by $2 * \pi$ and is the brown colored element in 9. It can be partly be inserted into a hole of the swing from above and is dimensioned one tenth of a millimetre smaller than the hole. The spring-loaded thrust piece inside the swing element interacts with the rotating element's notches. A notch has been placed evenly every $2 * \pi / 8$ to allow the rotary element to be locked in place in eight configurations according to 5. In order to be able to fix the modified artificial anterior chamber in it, the rotary device has a corresponding feature. Its shape is similar to the negative of the tissue retainer's wings. Two elongated holes are also part of the fastening element in order to attach screws countered with nuts. These are intended to enable a simple and secure clamping connection of the tissue retainer after insertion of the anterior chamber into the rotary element. It enables assembly that requires hardly any fine motor skills, as the lock nuts are self-locking in the sides of the rotary element. To avoid contamination of the superstructure and the nanoindenter during manual adjustment of the locking device positions, a cylindrical hexagon socket was fitted. The selection of the respective position is to be made by manual

exertion force in order to turn the element with the help of an Allen key.

5) *Modified Artificial Anterior Chamber by Barron*: Barron's AAC is a state of the art device allowing for tightly sealed and secured cornea mounting preventing any damage to the endothelial side of the tissue. The commercially available AAC consists of three components enabling the fixation without twisting the cornea while tightening. As defined in the requirements the device holds two ports for volume and pressure application of air and liquids which again are led out laterally through two holes in the lowest, louvred part of the device. The modification was made to reduce its height. Thus, the lowest louvred part was turned off on the lathe and the hoses were transferred further up. The reduced anterior chamber was only simplified in the CAD model as shown in fig. 11. Here, the locking ring with bayonet catch as well as the tubes were omitted and only the sub-assembly of the tissue platform with the cornea remaining after turning was modelled in CAD.

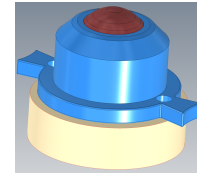


Fig. 11: Simplified CAD model of the height reduced Artificial Anterior Chamber with clamped cornea and tissue retainer.



Fig. 12: Illustration of the assembled prototype including the bayonet catch of the height reduced AAC.

E. Basic Functional Prototype Testing Results

It's possible to adjust the swing and the rotating element by hand, but the swing's locking positions can not be clearly recognised by hand alone. For the rotary element, however, the locking mechanism can be clearly recognised. Testing the devices for position adjustment by means of an Allen key showed, that it is possible to adjust the swing with it but rotating the rotary element is rather difficult and requires a lot of precise force, even when the spring loaded thrust piece was

removed from the swing. The checks of the locking function of the swing element inside the container in the three different positions showed, that the weight to be applied to the tissue retainer to overcome the locking force is at least 5.6 Newton as shown in table II.

TABLE II: Required weight in Newton to overcome the force of the locking mechanism by moving swing out of each configuration Pe, Pa and C1. For each position six measurements were carried out, the mean and standard deviation for the measured weight in kg converted into weight force in N is presented.

Measurement Nr.	Detent Position		
	Pe / N	Pa / N	C1 / N
1	5.6	8.98	16.42
2	6.77	10.61	14.53
3	5.66	12.54	16.98
4	6.19	11.5	17.48
5	6.3	12.2	16.4
6	6.4	9.58	15.27
Avg.	6.16	10.9	16.18
Mean	6.24	11.06	16.41
Std. Dev.	0.45	1.43	1.09

The container’s sealing property test resulted in an unchanged water level and no paper discoloration was noticed.

For the testing of usability the first issue identified was the transport from conventional laboratory to the nanoindenter site, as there was no covering lid present at that point. Also the insertion of the sample mount into the screwed on guide rail on the nanoindenter sample stage was tedious. The extensions of the original silicone tubes with Luer-Lock tube extensions laying freely in the sample mounts container resulted in an occasional block of the rotation element.

F. Preliminary whole human cornea Bioindentation Results

Three whole human corneal samples were characterized at two respective retrocorneal pressure levels of 20 and 40 mmHg. The test were performed before (ctrl) and after collagen cross-linking (CXL) as described in section II-C. Before CXL (ctrl) at 20 mmHg the three characterized corneas "Cornea 1", "Cornea 2" and "Cornea 3" show elastic moduli of 67.6 ± 4.3 , 89.9 ± 7.5 , 81.6 ± 6.5 kPa whereas they show 122.8 ± 4.1 , 130.6 ± 6.0 , 110.2 ± 6.5 kPa under cxl condition. At 40 mmHg the ctrl groups elastic moduli are 121.2 ± 6.8 , 155.9 ± 3.9 , 142.7 ± 6.1 kPa and increase to 162.1 ± 6.9 , 192.5 ± 3.6 , 166.4 ± 7.8 kPa after CXL treatment at the respective pressure level. The boxplots of the three corneas under these conditions are shown in fig. 13.

Grouping the data of the three corneas to pre- and post treatment, the histograms of the respective groups reveal several peaks under a spread width of up to 46 at the lower and 58 kPa at the higher pressure level. Due to the fact that the histogram does not clearly indicate a normal distribution, instead of a paired t-test the paired wilcoxon signed rank test was used for statistical analysis for both pressure levels. As shown in fig. 14 a significant increase in EM (p smaller than 0.001) was observed for both pressure levels.

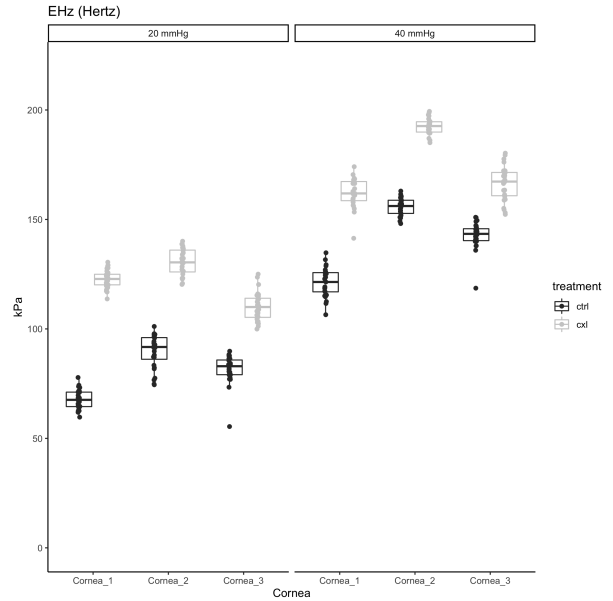


Fig. 13: Boxplots of effective modulus of three whole human cornea samples using Hertz fit at 20 and 40 mmHg retrocorneal pressure before and after treatment.

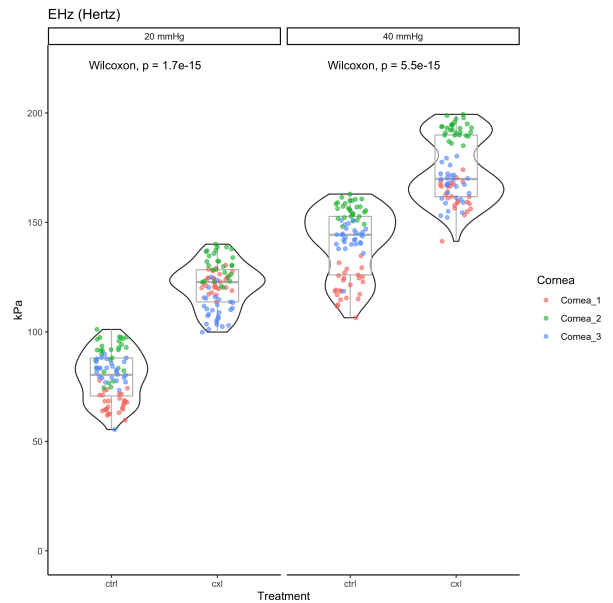


Fig. 14: Violin plot for the visualization of the three sample’s elasticity moduli pre- and post CXL treatment at both pressure levels of 20 and 40 mmHg with p-values indicating a significant increase in modulus (p smaller 0.001) obtained from paired wilcoxon signed rank tests.

IV. DISCUSSION AND SYSTEM EXTENSIONS FOR THE REVISED CONCEPT

The mechanism to move the rotatory element does not meet the required demands, which may be due to the one-sided lever arm on the one hand and the large friction surface on the other. Therefore, in the revision of the concept, a friction-reducing slide ring and a symmetrical tool for position adjustment have

been added. Also for the position adjustment of the swing, a symmetrical tool and device on the swing is added.

With regard to the more than four noticeable locking positions, it should first be noted that this condition is unacceptable for the intended use. It not only makes handling more difficult, but could potentially lead to incorrect measurements that may remain undetected. A possible reason for the observation could be that the slide rings of the swing have a misshapen surface, as the part was 3D printed hanging on its underside without any support structure. Thus, the unambiguous the locking position's readability is absolutely necessary to implement. For this purpose, Roman numerals have been attached to the inside of the container, which are positioned in such a way that the current position of the swing can be clearly identified. Although the execution of the hoses is done at a fixed position from the front chamber, a hemisphere was attached to the rotary element to indicate the set rotation position. The problems with insertion into the guide rail could be traced back to the spring-loaded thrust piece attached to the guide rails side. In order to prevent an incorrect screw-in depth, it is fixed with screw lock paste. The short silicone tubes of the modified artificial anterior chamber were replaced by longer tubes to avoid the use of mechanically blocking adapters.

Due to the defect of the UNHT³, it was not possible to perform indentations with the devised sample mount's prototype. Accordingly, the locking functions influence on the indentation response has not been tested with the UNHT³. However, the force exerted by the nanoindenter is much smaller than the force exerted by hand to change the locking position as shown the scale test confirmed.

With the immersed artificial anterior testing of central cornea area however, the other essential element of the concept could be verified. The tests have not only shown that indentations with the cornea clamped in an artificial anterior chamber are possible under the application of variable pressure, but also that the selected pressure has a remarkable influence on the modulus of the cornea.

Measuring deviations with the sample mount are inevitable, since the human cornea differs in its thickness, size and shape resulting in cornea samples never ideally matching with the simplified cornea model presented in III-B. Nevertheless, a way was sought to further reduce the measurement error due to geometric deviation. Since the natural shape of the donor tissue cannot and should not be changed, another option was sought. As shown in III-B2, the concept is based on the corneal high point being at the intersection of the two axes at the same time. This may be true for the CAD model, but due to the aforementioned deviations of the cornea, there may be a significant deviation in application. This in turn has the consequence that there is a deviation between the intended (cf. fig. 6) and the actual location of indentation for indentation radii greater than zero. In order to reduce the influence of different corneas heights resulting in the deviation from the two axis intersections, the system was expanded to include a height adjustment function. This shall enable the reduction of measurement error by ensuring the indentation of the desired positions. To do so, the swing element and also the rotary element were modified for the second revision, where a gauge

for cornea height adjustment was added. Several shims are used to raise or lower the cornea sitting the rotary element. This adaptation allows height adjustment in 0.1 mm steps and covers a height deviation range of up to 4 mm [2 mm higher or lower than perfect alignment position] leading to correction of the indentation position of up to 0.89 mm according to the CAD measurements presented in table III. The final sample mount is visualized in fig. 15 and an exploded view of an intermediate model is shown in fig. 16.

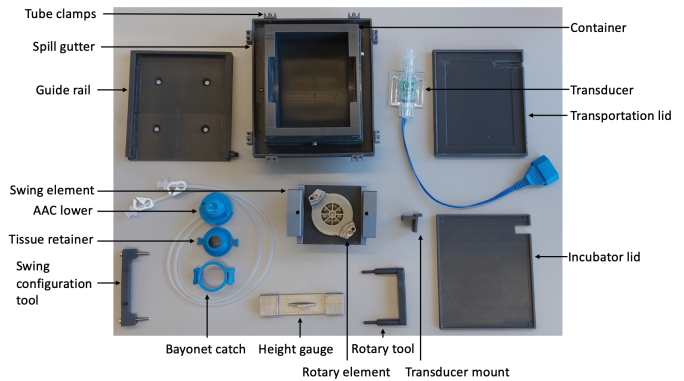


Fig. 15: Final sample mount and its respective components after remodeling. The fig. is showing the silicone hose clips mounted to the overflow protection rail, container, swing and rotary element, height reduced AAC, pressure transducer and respective attachment device, cornea height gauge, detent position adjustment tools, tight and untight lid.

TABLE III: Configuration-dependent horizontal distances between the indenter apex and the corresponding indentation point with two millimetre height displaced cornea and corresponding deviations from the desired indentation positions. The configurations refer to the respective configuration angle of the swing, where C0 refers to the configuration for central indentation right in the middle of the cornea's axis of rotation at the radius $c_0 = 0$ mm, C1 refers to the configuration for the indentation location on the radius $c_1 = 0.65$ mm and so on as explained in III-A

Configuration	Angle/deg	Distance/mm	Deviation/mm
C0	0	0	0
C1	4.8	0.73	0.17
Pa	15.6	2.01	0.54
Pe	26.3	3.7	0.89

V. CONCLUSION

A sample mount has successfully been developed enabling the indentation of whole corneal tissue. With it, it's possible to exert and maintain physiological conditions like the retrocorneal pressure or volume flow through an adapted artificial anterior chamber. The developed sample mount has been evaluated by several tests, which results described in III-E indicated several minor flaws and showed improvement potential, which were successfully revised as described in section IV. Due to a technical defect, the prototype could not be used with the UNHT³, as the space available has

been reduced by means of a short-term repair, which is why no indentations with the sample mount could be performed. Nevertheless, the weight measurement test results showed that the required forces to move the locking device are greater by a multiple of two powers than the exerted forces of the UNHT³ and the immersed artificial anterior chamber indentation test in the center of the cornea indicate a general proof of concept. In addition, with this novel approach a statistically significant difference between before and after collagen cross-linking treatment was demonstrated in the structure.

However, it is still difficult to estimate what the future holds for the sample mount, but as lied out in I-B the potential appears to be far reaching. The evaluation of different riboflavin protocols and irradiation durations assessment is the most presumable next step with many more yet to come.

APPENDIX A

EXPLODED DRAWING OF THE REVISED SAMPLE MOUNT

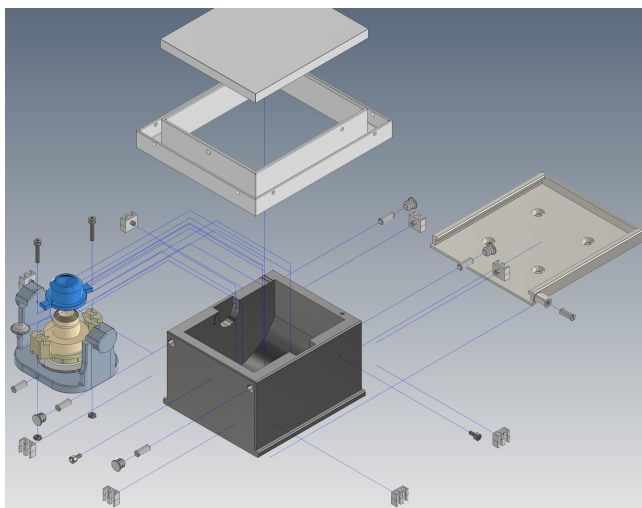


Fig. 16: Exploded Drawing of intermediate sample mount version



Fig. 17: YouTube QR Link to Explosion Drawing Video of Intermediate ample Mount Version

ACKNOWLEDGMENT

The author thanks the laboratory director Prof. Dr. med. Günther Schlunck and especially PD S. Lang for the supervision, help and tutorials enabling the success of the Thesis. The team spirit and willingness to help should be mentioned in particular, which the management lives out in an exemplary manner leading to a pleasant and motivating working atmosphere. Special thanks goes to R. Lohmüller for providing great, comprehensive familiarisation into the new environment and his great support in the trial implementation.

Furthermore, thanks go to the workshop manager P. Weisert for the manufacturing and also to all unnamed colleagues for their help with any questions.

REFERENCES

- [1] L. Qian and H. Zhao, "Nanoindentation of soft biological materials," dec 2018. [Online]. Available: <https://www.mdpi.com/2072-666X/9/12/654/htm>
- [2] A. A. Zadpoor, "Mechanics of biological tissues and biomaterials: Current trends," *Materials (Basel)*, vol. 8, no. 7, pp. 4505–4511, 2015.
- [3] S. Huang and D. E. Ingber, "Cell tension, matrix mechanics, and cancer development," *Cancer Cell*, vol. 8, no. 3, pp. 175–176, 2005.
- [4] S. Garcia-Manyes, O. Domènech, F. Sanz, M. T. Montero, and J. Hernandez-Borrell, "Atomic force microscopy and force spectroscopy study of Langmuir-Blodgett films formed by heteroacid phospholipids of biological interest," *Biochim. Biophys. Acta - Biomembr.*, vol. 1768, no. 5, pp. 1190–1198, 2007.
- [5] A. J. Engler, S. Sen, H. L. Sweeney, and D. E. Discher, "Matrix Elasticity Directs Stem Cell Lineage Specification," *Cell*, vol. 126, no. 4, pp. 677–689, 2006.
- [6] M. V. Swain, J. Nohava, and P. Eberwein, "A simple basis for determination of the modulus and hydraulic conductivity of human ocular surface using nano-indentation," *Acta Biomater.*, vol. 50, pp. 312–321, mar 2017.
- [7] J. Nohava, M. Swain, S. J. Lang, P. Maier, S. Heinzlmann, T. Reinhard, and P. Eberwein, "Instrumented indentation for determination of mechanical properties of human cornea after ultraviolet-A crosslinking," *J. Biomed. Mater. Res. - Part A*, vol. 106, no. 5, pp. 1413–1420, may 2018.
- [8] M. L. Oyen, "Nanoindentation of hydrated materials and tissues," *Curr. Opin. Solid State Mater. Sci.*, vol. 19, no. 6, pp. 317–323, 2015. [Online]. Available: <http://dx.doi.org/10.1016/j.cossms.2015.03.001>
- [9] L. Qian, H. Zhao, Y. Guo, Y. Li, M. Zhou, L. Yang, Z. Wang, and Y. Sun, "Influence of strain rate on indentation response of porcine brain," *J. Mech. Behav. Biomed. Mater.*, vol. 82, pp. 210–217, 2018. [Online]. Available: <https://doi.org/10.1016/j.jmbm.2018.03.031>
- [10] C. T. McKee, J. A. Last, P. Russell, and C. J. Murphy, "Indentation versus tensile measurements of young's modulus for soft biological tissues," *Tissue Eng. - Part B Rev.*, vol. 17, no. 3, pp. 155–164, 2011.
- [11] J. Seifert, C. M. Hammer, J. Rheinlaender, S. Sel, M. Scholz, F. Paulsen, and T. E. Schäffer, "Distribution of young's modulus in porcine corneas after riboflavin/UVA-induced collagen cross-linking as measured by atomic force microscopy," *PLoS One*, vol. 9, no. 1, pp. 1–8, 2014.
- [12] J. A. Last, S. J. Liliensiek, P. F. Nealey, and C. J. Murphy, "Determining the mechanical properties of human corneal basement membranes with atomic force microscopy," *J. Struct. Biol.*, vol. 167, no. 1, pp. 19–24, 2009. [Online]. Available: <http://dx.doi.org/10.1016/j.jsb.2009.03.012>
- [13] M. L. Oyen, T. A. Shean, D. G. Strange, and M. Galli, "Size effects in indentation of hydrated biological tissues," *J. Mater. Res.*, vol. 27, no. 1, pp. 245–255, 2012.
- [14] A. Bergua, *Das menschliche Auge in Zahlen*. Springer Berlin Heidelberg, 2017.
- [15] Heinrich Kipp, "K0309 Inch - Spring Plungers ball style - Spring Plungers ball style, slotted, steel, standard end pressure, inch," p. 2, 2021. [Online]. Available: https://www.kippusa.com/xs_db/DOKUMENT_DB/www/KIPP_US/BEDIENTEILE/DataSheet/enUS/K03/K0309_Inch_Datasheet_11035_Spring_Plungers_ball_style_slotted_steel_standard_end_pressure_inch-enUS.pdf

Bero Bressler is student of the Medical Technologies Master program at Management Center Innsbruck, Tirol, Austria. In corporation with the Universitätsklinikum Freiburg he wrote his Thesis under supervision of PD Dr. med. S.J. Lang in the clinic's experimental ophthalmology department.

